

3 Seismic interferometry in the presence of an isolated 4 noise source

5 **S. Schippkus *¹, R. Snieder², C. Hadzioannou¹**

6 ¹Institute of Geophysics, Centre for Earth System Research and Sustainability (CEN), Universität Hamburg, Hamburg, Germany, ²Center
7 for Wave Phenomena, Colorado School of Mines, Boulder, CO, USA

Abstract

8 Seismic interferometry gives rise to a correlation wavefield that is closely related to
the Green's function under the assumption of uniformly distributed noise sources. In the
presence of an additional isolated noise source, a second contribution to this wavefield is
introduced that emerges from the isolated source location at negative lapse time. These
two contributions interfere, which may bias surface wave dispersion measurements sig-
nificantly. To avoid bias, the causal and acausal parts of correlation functions need to be
treated separately. We illustrate this by applying seismic interferometry to field data from
a large-N array where a wind farm is present within the array.

9 1 Introduction

10 Seismic interferometry is a well-established technique to estimate wavefields propagating between pairs of stations
11 from recordings of ambient seismic noise (Nakata et al., 2019, and references therein). These wavefields are com-
12 monly used to image (e.g., Lin et al., 2008; de Ridder and Biondi, 2015; Schippkus et al., 2018) and monitor (e.g.,
13 Wegler and Sens-Schönfelder, 2007; Brenguier et al., 2008; Steinmann et al., 2021) Earth's structure. For a uniform
14 distribution of uncorrelated noise sources, the wavefield that emerges from cross-correlation of seismic records be-
15 tween two stations is closely related to the Green's function between them. This relation may be derived by assuming
16 a diffuse wavefield (Lobkis and Weaver, 2001), equipartition of energy across surface wave modes (Weaver, 2010), or
17 sources on a boundary surrounding the two stations (Wapenaar et al., 2005).

18 In this study, we investigate the case where the presence of an additional isolated source violates these assump-
19 tions and introduces an additional contribution to cross-correlation functions. In the following, we demonstrate the
20 isolated-source contribution using data from a large-N deployment in the Vienna basin, Austria, derive the expected
21 behaviour of this contribution, compare our predictions with observations from the large array, and explore what
22 impact the second contribution may have in practice.

23 2 Cross-correlation of the recorded wavefield

24 We use data from 4907 seismic stations with \sim 200m inter-station spacing in the Vienna basin, Austria (Fig. 1). Stations
25 were deployed in March 2019 as part of a seismic exploration survey by OMV E&P GmbH and recorded data contin-
26 uously over four weeks. This deployment is similar to the one described in Schippkus et al. (2020), with comparable
27 instruments (several co-located 10Hz-geophones per station) and in an area that is partly overlapping with the pre-
28 vious deployment towards the Southeast. Therefore, the same sources of seismic noise characterised by Schippkus
29 et al. (2020) are also present in this data: wind farms, railway tracks, roads, and oil pumpjacks, among others.

30 Schippkus et al. (2020) already hinted at the potential impact of strong isolated sources on correlation functions
31 in this region. To investigate the sources' impact, we compute cross correlations between all stations and a master
32 station at location r_M in the center of the deployment (Fig. 2a). The seismograms were spectrally whitened and cut
33 into 1hr-windows before cross-correlation, stacked linearly after cross-correlation, and bandpass-filtered from 0.5 to
34 1.0 Hz. A movie of correlation function amplitudes over time is provided in the electronic supplementary material.

35 Figure 2 and the movie show two distinct contributions to the correlation wavefield. First, a contribution con-
36 verging onto the master station r_M at acausal lapse times $\tau < 0$ and diverging at causal lapse times $\tau > 0$ (Fig. 2a).
37 This is the expected behaviour that commonly arises from seismic interferometry under the assumptions described

*Corresponding author: sven.schippkus@uni-hamburg.de

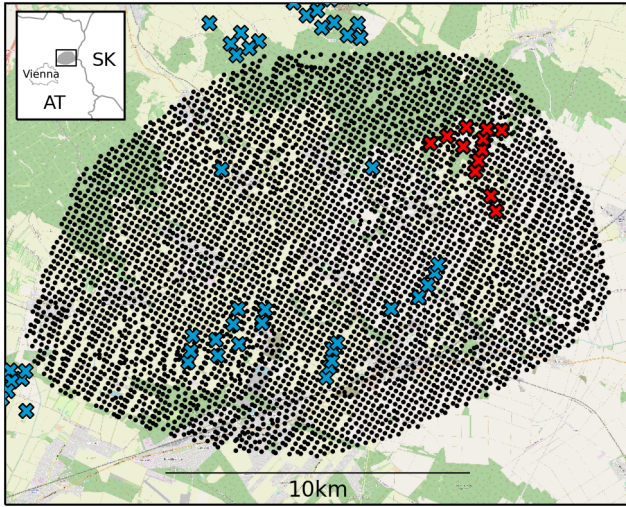


Figure 1 Map of the study area. 4907 seismic stations (black dots) Northeast of Vienna, near the Austrian-Slovakian border. Wind turbines in the wind farm Prottes-Ollersdorf are marked with red crosses; blue crosses mark all other wind turbines.

above (e.g., Lin et al., 2008). In addition, there is a second contribution emerging from a location \mathbf{r}_N in the Northeast of the deployment at $\tau \approx -12$ sec. that propagates only outwards from \mathbf{r}_N . The center of this wavefield contribution coincides with the location of the wind farm Prottes-Ollersdorf (Fig. 1), the strongest and most consistent source of anthropogenic noise in the region (Schippkus et al., 2020). In the next section, we derive the behaviour of this contribution to the cross correlations.

3 Cross-correlation in the presence of an isolated noise source

We consider a wavefield that is generated by a combination noise sources on a boundary surrounding the array and an isolated noise source within the boundary with noise spectrum $N_I(\omega)$ at location \mathbf{r}_N (Fig. 2). The treatment of this section is formulated in the frequency domain. We assume that the noise sources on the boundary have equal power spectrum $|N_B|^2$, and that the noise generated at different locations are uncorrelated. This means that

$$\langle N_B(\mathbf{r}')N_B^*(\mathbf{r}'') \rangle = |N_B|^2 \delta(\mathbf{r}' - \mathbf{r}'') , \quad (1)$$

where $\langle \dots \rangle$ denotes the expectation value. We also assume that the noise on the boundary and the noise from the isolated noise source with spectrum N_I is uncorrelated, hence

$$\langle N_B(\mathbf{r}')N_I^*(\mathbf{r}'') \rangle = \langle N_I N_B^*(\mathbf{r}') \rangle = 0 . \quad (2)$$

The wavefield is excited by the superposition of noise sources at the boundary and the isolated noise source, hence

$$u(\mathbf{r}) = \oint G(\mathbf{r}, \mathbf{r}') N_B(\mathbf{r}') dS' + G(\mathbf{r}, \mathbf{r}_N) N_I . \quad (3)$$

The cross correlation of the wavefield at location \mathbf{r} with the wavefield at the master station at \mathbf{r}_M is given by

$$\begin{aligned} \langle u(\mathbf{r})u^*(\mathbf{r}_M) \rangle &= \oint \oint G(\mathbf{r}, \mathbf{r}') G^*(\mathbf{r}_M, \mathbf{r}'') \langle N_B(\mathbf{r}') N_B(\mathbf{r}'') \rangle dS' dS'' \\ &+ \oint G(\mathbf{r}, \mathbf{r}') G^*(\mathbf{r}_M, \mathbf{r}_N) \langle N_B(\mathbf{r}') N_I^* \rangle dS' + \oint G(\mathbf{r}, \mathbf{r}_N) G^*(\mathbf{r}_M, \mathbf{r}') \langle N_I N_B^*(\mathbf{r}') \rangle dS' \\ &+ G(\mathbf{r}, \mathbf{r}_N) G^*(\mathbf{r}_M, \mathbf{r}_N) |N_I|^2 . \end{aligned} \quad (4)$$

Because of expression (1) the double integral in the first term reduces to a single integral, and because of equation (2) the second and the third term in equation (4) vanish, hence

$$\langle u(\mathbf{r})u^*(\mathbf{r}_M) \rangle = \oint G(\mathbf{r}, \mathbf{r}') G^*(\mathbf{r}_M, \mathbf{r}') dS' |N_B|^2 + G(\mathbf{r}, \mathbf{r}_N) G^*(\mathbf{r}_M, \mathbf{r}_N) |N_I|^2 . \quad (5)$$

Note the symmetry between the contribution of the surface sources and the contribution of the isolated source.

The surface integral in the first term can be rewritten using equation (11) of Wapenaar et al. (2005), which in the notation of this paper is given by $G(\mathbf{r}, \mathbf{r}_M) + G^*(\mathbf{r}, \mathbf{r}_M) = (2/\rho c) \oint G(\mathbf{r}, \mathbf{r}') G^*(\mathbf{r}_M, \mathbf{r}') dS'$, hence equation (5) can be written as

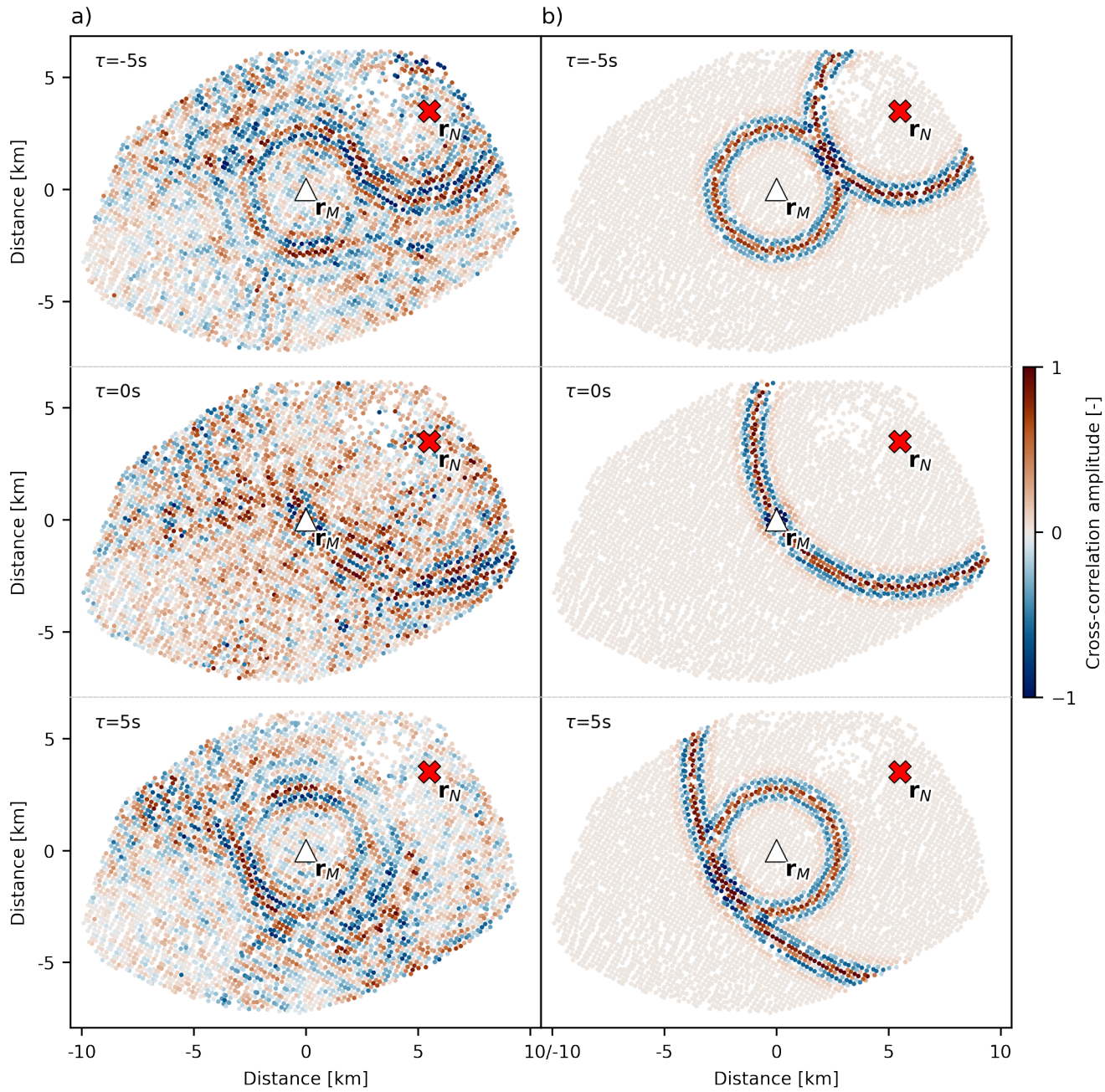


Figure 2 Snapshots of cross-correlation function amplitudes in the presence of an isolated source at different lapse times $\tau = [-5, 0, 5]$ sec. The white triangle marks the master station r_M , the red cross marks the approximate location of the isolated source r_N . a) Correlation functions from four weeks of data, bandpass-filtered from 0.5 to 1.0Hz. The isolated source induces a contribution centered on r_N . b) Modelled correlation functions for the two contributions by sources on a boundary and by the isolated source (eq. 9) predict the observations.

$$\langle u(\mathbf{r})u^*(\mathbf{r}_M) \rangle = \frac{\rho c |N_B|^2}{2} (G(\mathbf{r}, \mathbf{r}_M) + G^*(\mathbf{r}, \mathbf{r}_M)) + |N_I|^2 G(\mathbf{r}, \mathbf{r}_N) G^*(\mathbf{r}_M, \mathbf{r}_N). \quad (6)$$

The first term on the right hand denotes the superposition of the Green's function and its time-reversed counterpart. These terms usually arise in seismic interferometry. The second term on the right hand side describes an additional contribution to the cross-correlation of the wavefield that is caused by the isolated noise source. We analyse the kinematics of this term in the next section.

4 Kinematics of the isolated noise source's contribution

The surface wave Green's function is, in the far field, proportional to

$$G(\mathbf{r}, \mathbf{r}_N) \propto e^{i(k|\mathbf{r}-\mathbf{r}_N|+\pi/4)}, \quad (7)$$

with wavenumber k (Aki and Richards, 2002). Thus, in the far field the last term in expression (6) satisfies

$$|N_I|^2 G(\mathbf{r}, \mathbf{r}_N) G^*(\mathbf{r}_M, \mathbf{r}_N) \propto |N_I|^2 e^{ik(|\mathbf{r}-\mathbf{r}_N|-|\mathbf{r}_M-\mathbf{r}_N|)}, \quad (8)$$

which gives an arrival at lapse time

$$\tau(\mathbf{r}) = \frac{|\mathbf{r}-\mathbf{r}_N|}{c} - \frac{|\mathbf{r}_M-\mathbf{r}_N|}{c}, \quad (9)$$

for medium velocity c . Note that for a given master station $|\mathbf{r}_M - \mathbf{r}_N|/c = \text{constant}$. Equation (9) shows that all locations \mathbf{r} with the same distance to \mathbf{r}_N have the same arrival time $\tau(\mathbf{r})$; the travel time of the contribution to the correlation wavefield induced by the isolated source is constant on a circle centered on \mathbf{r}_N . This contribution emerges from \mathbf{r}_N at

$$\tau(\mathbf{r} = \mathbf{r}_N) = -\frac{|\mathbf{r}_M - \mathbf{r}_N|}{c}, \quad (10)$$

and reaches the master station at $\tau(\mathbf{r} = \mathbf{r}_M) = 0$.

To understand the relation between the waveforms described by the first term of equation (6) and the additional term, we analyze the arrival time of these waves on a line from \mathbf{r}_M to \mathbf{r}_N . Take the x -axis to point in the positive direction from \mathbf{r}_M to \mathbf{r}_N and consider points on the line between these locations, hence $x_M < x < x_N$. For a given location x , the acausal wave described by the term $G^*(\mathbf{r}, \mathbf{r}_M)$ gives an arrival at time $t = -|\mathbf{r} - \mathbf{r}_M|/c = -(x - x_M)/c$. This means that for a given time t , the acausal direct wave is located at

$$x_{dir} = x_M - ct. \quad (11)$$

(Note that since $t < 0$, $x > x_M$.) The additional arrival due to the isolated noise source gives for a location x according to expression (9) an arrival at $t = |x_N - x|/c + |x_N - x_M|/c = -(x - x_M)/c$, so that for a given time t the wave is at location

$$x_{add} = x_M - ct. \quad (12)$$

This means that for a time t the wavefronts from the acausal direct wave and the contribution from the isolated noise source are at the same location at the line from \mathbf{r}_M to \mathbf{r}_N . Geometrically speaking, the incoming wave to \mathbf{r}_M and the outgoing wave from \mathbf{r}_N touch at the line from \mathbf{r}_M to \mathbf{r}_N . Similarly, the contribution by the isolated noise source touches the causal wave described by the term $G(\mathbf{r}, \mathbf{r}_M)$ for locations $x < x_M$. This behavior is confirmed by the touching wavefronts in Figure 2 and the movie. Note that there is no acausal contribution in the second term of expression (6), because the original wavefield induced at \mathbf{r}_N only propagates in one direction (away from \mathbf{r}_N), in contrast to the wavefield emitted at the boundary, which propagates in all directions. Therefore, the isolated source's contribution to the correlation wavefield has no energy at $\tau(\mathbf{r}) < -|\mathbf{r}_M - \mathbf{r}_N|/c$.

We model the described kinematics and compare against our observations (Fig. 2). We approximate the wind farm Prottes-Ollersdorf as a single source and assume that both the boundary sources and the isolated source emit the same Ricker wavelets. For demonstration purposes, we assume a constant medium velocity $c \approx 550$ m/s, estimated from the time the isolated-source contribution emerges $\tau(\mathbf{r} = \mathbf{r}_N)$ and the distance $|\mathbf{r}_M - \mathbf{r}_N|$. Our model explains the observed contributions to the correlation wavefield.

5 Velocity measurement errors due to interference

Because the wavefronts from the two contributions touch and have the same wavelengths, they interfere. Along the line connecting \mathbf{r}_N and \mathbf{r}_M they are exactly in phase, and show varying degrees of constructive and destructive interference away from this line (Fig. 2). This behaviour implies that measurements on cross-correlation functions may be adversely affected in the presence of an isolated source for station pairs not on this line. In a standard ambient noise tomography application, travel times of seismic waves are measured between all station pairs from correlation functions and inverted for maps of seismic wave speed.

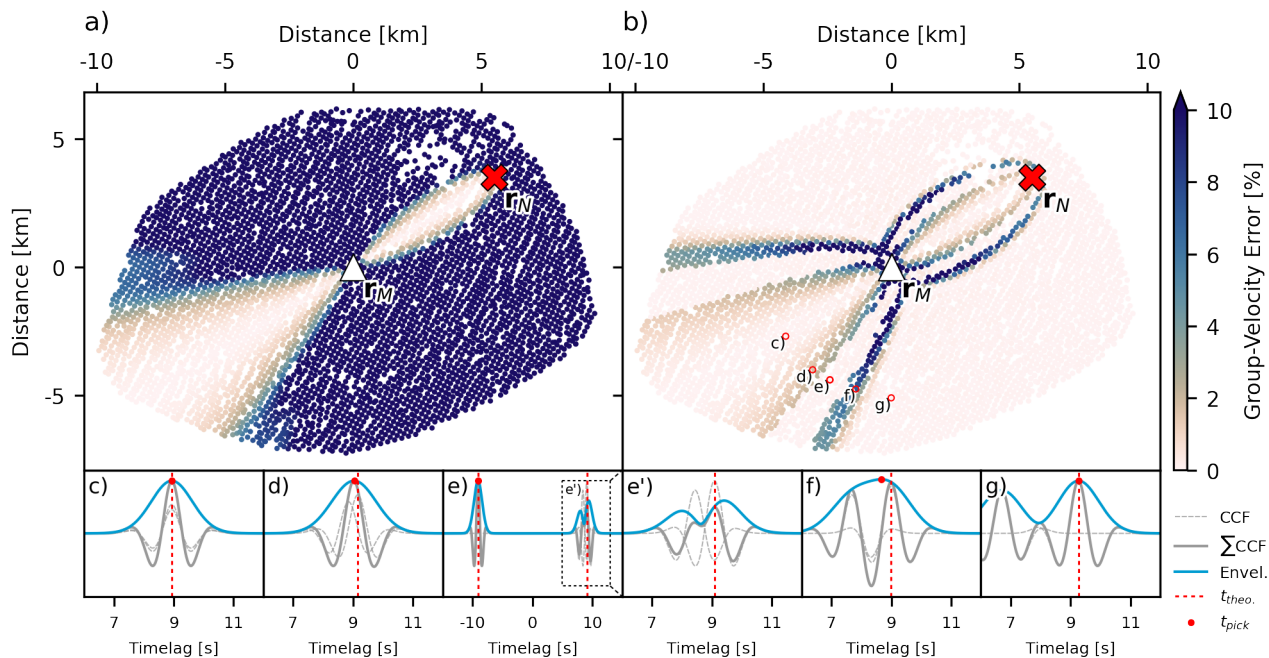


Figure 3 Group-velocity measurement errors due to the interference between the two contributions to the correlation wavefield. We cap the colormap at 10% error for illustration purposes. a) Errors if the correlation wavefield induced by the isolated source r_N has higher amplitudes. Interference of the two contributions results in significant measurement errors away from the line connecting r_N and r_M . b) Errors if the correlation wavefield induced by the sources on the boundary has higher amplitudes. Significant errors due to interference. c-g) Picked group arrivals on correlation functions for b). These show correlation function contributions by the two types of sources (dashed grey lines), sum of the two contributions (thick grey line), the sum's envelope (blue line), theoretical arrival time (red dashed line), and picked arrival time (red dot). Note the wider time window in e) and its zoom-in e').

We demonstrate the impact the isolated source has on such measurements by measuring group travel times from the modelled correlation functions (Fig. 2b). From these measurements we compute relative group-velocity measurement errors (Fig. 3). Two cases are investigated: one where the isolated source induces a contribution in the correlation wavefield with 25% higher amplitudes than the contribution due to sources on the boundary (Fig. 3a), and one where the boundary sources produce the stronger contribution (also 25%, Fig. 3b).

In the first case, the measurement errors vanish only along the line connecting r_N and r_M where the two contributions are in phase (Fig. 3a). Away from this line, measurement errors increase to infinity (apparent travel times of 0) for stations r with $|r - r_N| = |r_M - r_N|$. In practice, velocity measurements deviating significantly from expected values are commonly classified as outliers or attributed to spurious arrivals and discarded. Our results show that measurement errors of at least 10% occur for the majority of station pairs in the case of a stronger isolated source.

In the case of a weaker isolated source, we find a distinct pattern of measurement errors of several percent (Fig. 3b). Such measurement errors would likely not be identified as clear outliers or spurious arrivals and could bias results. To illustrate why this pattern occurs, we show the group travel time measurements at five stations (Fig. 3e-g, red circles in Fig. 3b). Starting at the line connecting r_N and r_M , we find that both contributions are in phase, resulting in no error (Fig. 3c). As we increase distance to this line, a slight shift between the two contributions shifts the envelope's peak towards lower lapse time, resulting in a higher-velocity estimate (Fig. 3d). This error increases until another band with zero error (Fig. 3e). This band exists, because destructive interference decreases amplitudes to values lower than the acausal part of the correlation function, which is caused only by the boundary sources at this location. The travel time is then automatically picked on the acausal side where no interference occurs (Fig. 3e). If the travel time was picked in the causal part instead, interference would result in negative velocity errors (zoom-in in Fig. 3e'). At a certain distance, the two contributions interfere constructively again (Fig. 3f), resulting in a bias similar to the case in Figure 3d. Finally, as the two wavefields separate, no interference occurs and the envelope of the stronger contribution to the correlation wavefield is picked; in this case the contribution of the boundary sources (Fig. 3g). This also explains the behaviour in the first case, where the isolated source dominates the measurement away from the line simply due to higher amplitudes.

The distribution of errors for both cases depends on relative amplitudes of the two contributions, source terms, frequency range, and the locations of r_M and r_N . With knowledge of these factors, measurement errors can be avoided. One straightforward strategy is to avoid measuring where interference occurs by selecting which side of the correlation functions to measure on – depending on the geometry of r , r_N and r_M – in combination with a windowing function around expected arrival times. In the case of a stronger contribution by the boundary sources (Fig. 3b)

129 selecting the side of the correlation function without interference is sufficient (Suppl. Fig. S1b). In the case of a
 130 strong isolated source, an additional windowing function is necessary (Suppl. Figs. S2, S3). See supplementary
 131 material for more details.

132 6 Discussion

133 We describe the contribution of an isolated noise source to the cross-correlation wavefield in seismic interferometry
 134 and how it relates to the contribution by boundary sources. Our derivation predicts the observed correlation
 135 wavefield, and this is the first time both contributions are clearly recovered simultaneously (Fig. 2). In the following,
 136 we discuss the implications our results have for studies based on seismic interferometry and how this work may be
 137 expanded upon in the future.

138 The dataset in this study is not the first to record isolated noise sources that are used the context of seismic in-
 139 terferometry. [Droznin et al. \(2015\)](#) used cross-correlation of continuous recordings of volcanic tremor to estimate
 140 their location. [Dales et al. \(2017\)](#) exploited the correlation wavefield contribution from continuously operating ore
 141 crushers for monitoring of an underground mine. [Brenguier et al. \(2019\)](#) proposed to use body waves from train
 142 signals excited in the stationary phase of two arrays for structural monitoring of a fault between the two arrays. The
 143 crucial feature these sources have in common is that they excite seismic energy repeatedly, similar to the wind farm
 144 in our dataset. In previous studies that use such sources, the correlation wavefield has been dominated by the iso-
 145 lated sources' contribution, masking the contribution by boundary sources ([Droznin et al., 2015](#); [Dales et al., 2017](#);
 146 [Brenguier et al., 2019](#)).

147 In this study, we recover the two different contributions to the correlation wavefield simultaneously. Expression
 148 (6) shows that for both contributions to the correlation wavefield to have comparable amplitudes, the source terms
 149 must have the "right" ratio of energy. For our data, both contributions emerge clearly only with spectral whitening
 150 applied, i.e., normalisation of energy across frequencies. Without spectral whitening, the correlation wavefield is
 151 dominated by the contribution of the wind farm Prottens-Ollersdorf, similar to how the 26s microseism biases corre-
 152 lation functions in [Bensen et al. \(2007\)](#). It is likely that whitening is successful on our data, because wind turbines
 153 excite seismic energy most effectively at specific frequencies related to the eigenmodes of the wind turbine towers,
 154 whereas other sources of ambient noise in the region excite energy over a wider frequency range at lower energy
 155 levels ([Schippkus et al., 2020](#)). Normalising the energy levels across frequencies changes their relative strength to
 156 be comparable in the wideband correlation functions we investigate here. Additional contributions to the corre-
 157 lation wavefield may in principle also occur at lower frequencies where the presence of isolated sources is usually not
 158 considered, e.g., near the secondary microseism band.

159 There is significant variation in each contribution's amplitudes at different receiver locations r , which our mod-
 160 ellelling does not incorporate (Fig. 2). Among the potential reasons for this are coupling of geophones into the ground,
 161 local amplification and attenuation effects, or a non-uniform excitation pattern by the wind farm. Ultimately, we are
 162 only able to clearly identify and distinguish the two different contributions thanks to high spatial sampling of the
 163 correlation wavefield and its coherency across stations. This is also the likely reason we are the first to identify this
 164 behaviour in data, as we would have probably missed it with significantly fewer stations.

165 Signals that arrive before the expected direct wave in correlation functions are often attributed to unphysical or
 166 "spurious" arrivals ([Snieder et al., 2006, 2008](#)). These emerge from uncancelled cross terms in correlation functions
 167 and can be exploited ([Colombi et al., 2014; Retailleau et al., 2017; Li et al., 2020](#)). The signal due to the isolated source
 168 has also arrives before or concurrent with the direct waves of the boundary source contribution, but it is physical
 169 instead. It results neither from cross terms of boundary sources with themselves (eq. 1) nor from uncancelled cross
 170 terms of the boundary sources and isolated source (eq. 2). We have shown in our analysis that this contribution can
 171 have significant impact on travel-time measurements (Fig. 3), which may be missed if one is unaware of the presence
 172 of an isolated source. This applies in a similar manner to measurements of amplitudes or phase velocities.

173 The basic approach we propose to avoid travel-time measurement errors requires a nearly symmetric contribu-
 174 tion to the correlation wavefield by the boundary sources, i.e., an even distribution of boundary sources ([Snieder
 175 et al., 2008](#)). In real-world applications, strongly asymmetric correlation functions with sufficient signal-to-noise ra-
 176 tio on only one side are common (e.g., [Brenguier et al., 2008; Retailleau et al., 2017; Schippkus et al., 2018](#)). If that
 177 side also is the side that contains the contribution by the isolated source, our proposed strategy is not applicable. In
 178 the context of tomography, one may still achieve sufficient coverage of measurements when applying a windowing
 179 function. Related to this, the causal and acausal parts of correlation functions are often stacked ("folded") to increase
 180 signal-to-noise ratio (e.g., [Lin et al., 2008; de Ridder and Biondi, 2015; Schippkus et al., 2018](#)). In the presence of an
 181 isolated noise source, folding correlations effectively forces the asymmetric contribution of the isolated source to
 182 become symmetric. This prevents the basic strategy for avoiding measurement errors described above and results
 183 in additional interference. In the case of an isolated noise source, we strongly advise against folding correlations.

184 Isolated noise sources may also have significant implications for monitoring applications that exploit the coda
 185 of correlation functions. While the direct waves of both contributions to the correlation wavefield only interfere for
 186 certain station pair geometries (Fig. 2), coda waves of both contributions can overlap and interfere for a larger range
 187 of geometries. This could induce apparent velocity changes simply due to changes in the strength of the isolated
 188 source over time, similar to how velocity measurement errors on the direct wave depend on relative amplitude (Fig.

189 3). However, this would also be accompanied by a drop in correlation coefficient, which can indicate a change in
 190 source distribution and is often used as a quality criterion (e.g., [Wegler and Sens-Schönfelder, 2007](#)). Additionally,
 191 the origin of the coda wavefield dictates its spatial sensitivity ([Margerin et al., 2016](#)). If the origin is misattributed,
 192 it may lead to misinterpretation of results. Similar to the strategy for travel-time measurements described above,
 193 careful coda window selection, based on the asymmetry of the isolated source contribution, may help avoid these
 194 effects also for monitoring applications.

195 We treat the wind farm Prottes-Ollersdorf as a single source in our derivation and modelling (Fig. 2). When
 196 considering multiple isolated noise sources, the derivation straightforwardly gives rise to a single contribution for
 197 each of those sources, assuming they are uncorrelated. Indeed, when we consider each wind turbine in the wind farm
 198 separately, the fit with observed correlation functions improves (Fig. S4). This suggests that knowledge about the
 199 presence and characteristics of isolated sources may be used to remove their contributions and achieve correlation
 200 functions that are less impacted by local sources.

201 In our analysis, we have only considered vertical components, because only vertical component recordings are
 202 available in our dataset. Because the two contributions to the correlation wavefield propagate in different directions
 203 for some station pairs, questions arise about the interaction between differently polarised wave types with different
 204 velocities when analysing horizontal component recordings, i.e., potential interference of Love and Rayleigh waves.
 205 They may not be well-separated and interfere to affect measurements, similar to the above. Defining an appropriate
 206 windowing function may prove more difficult in that case. The case of horizontal components is a potential target
 207 for future works.

208 We demonstrate that different contributions to the correlation wavefield can carry similar energy and interfere.
 209 In previous studies, isolated noise sources have dominated the correlation wavefield, whereas we present a case
 210 where the contribution by boundary sources and by isolated sources have similar amplitudes, which leads to biased
 211 travel-time measurements. Ideally, studies that rely on seismic interferometry should always consider the possibility
 212 of isolated noise sources in their data and how such sources may impact results, especially at frequencies where
 213 anthropogenic sources dominate.

214 Data Availability and Resources

215 Seismograms used in this study were collected using an array for industrial exploration by OMV E&P GmbH. Due
 216 to a non-disclosure agreement with OMV E&P GmbH, the authors cannot make this data publicly available. The
 217 supplemental material includes a movie of cross-correlation function amplitudes over time, more details on the
 218 proposed strategy to avoid measurement errors, and the case when multiple isolated noise sources are considered.
 219 Colormaps used for illustrations are perceptually uniform ([Crameri, 2021](#)).

220 Acknowledgements

221 The authors thank OMV E&P GmbH for granting access to the seismic data. [SPIN]. This research was partially funded
 222 by the Federal Ministry of Education and Research (BMBF) and the Free and Hanseatic City of Hamburg under the
 223 Excellence Strategy of the Federal Government and the Länder. This work was partially funded by the Emmy Noether
 224 program (HA7019/1-1) of the German Research Foundation (DFG). This work was partially funded by the European
 225 Union's Horizon 2020 research and innovation programme under the Marie Skłodowska-Curie grant agreement No.
 226 955515.

227 References

- 228 Aki, K. and Richards, P. *Quantitative Seismology*. Univ. Science Books, Sausalito, second edition, 2002.
- 229 Bensen, G. D., Ritzwoller, M. H., Barmin, M. P., Levshin, A. L., Lin, F., Moschetti, M. P., Shapiro, N. M., and Yang, Y. Processing seismic ambient
 noise data to obtain reliable broad-band surface wave dispersion measurements. *Geophysical Journal International*, 169(3):1239–1260,
 June 2007. doi: [10.1111/j.1365-246X.2007.03374.x](https://doi.org/10.1111/j.1365-246X.2007.03374.x).
- 232 Brenguier, F., Campillo, M., Hadzioannou, C., Shapiro, N. M., Nadeau, R. M., and Larose, E. Postseismic relaxation along the San
 Andreas fault at Parkfield from continuous seismological observations. *Science (New York, N.Y.)*, 321(5895):1478–1481, Sept. 2008.
 doi: [10.1126/science.1160943](https://doi.org/10.1126/science.1160943).
- 235 Brenguier, F., Boué, P., Ben-Zion, Y., Vernon, F. L., Johnson, C. W., Mordret, A., Coutant, O., Share, P. E., Beaucé, E., Hollis, D., and Lecocq,
 T. Train traffic as a powerful noise source for monitoring active faults with seismic interferometry. *Geophysical Research Letters*, 46(16):
 9529–9536, Aug. 2019. doi: [10.1029/2019GL083438](https://doi.org/10.1029/2019GL083438).
- 238 Colombi, A., Boschi, L., Roux, P., and Campillo, M. Green's function retrieval through cross-correlations in a two-dimensional complex
 reverberating medium. *The Journal of the Acoustical Society of America*, 135(3):1034–1043, Mar. 2014. doi: [10.1121/1.4864485](https://doi.org/10.1121/1.4864485).
- 240 Crameri, F. Scientific colour maps. Zenodo, Sept. 2021.
- 241 Dales, P., Audet, P., and Olivier, G. Seismic Interferometry Using Persistent Noise Sources for Temporal Subsurface Monitoring. *Geophysical
 Research Letters*, 44(21):10,863–10,870, 2017. doi: [10.1002/2017GL075342](https://doi.org/10.1002/2017GL075342).

- 243 de Ridder, S. A. L. and Biondi, B. L. Ambient seismic noise tomography at Ekofisk. *GEOPHYSICS*, 80(6):B167–B176, Nov. 2015.
244 doi: 10.1190/geo2014-0558.1.
- 245 Drozbin, D., Shapiro, N., Droznina, S. Y., Senyukov, S., Chebrov, V., and Gordeev, E. Detecting and locating volcanic tremors on the
246 Klyuchevskoy group of volcanoes (Kamchatka) based on correlations of continuous seismic records. *Geophysical Journal International*,
247 203(2):1001–1010, Nov. 2015. doi: 10.1093/gji/ggv342.
- 248 Li, L., Boué, P., and Campillo, M. Observation and explanation of spurious seismic signals emerging in teleseismic noise correlations. *Solid*
249 *Earth*, 11(1):173–184, 2020. doi: 10.5194/se-11-173-2020.
- 250 Lin, F.-C., Moschetti, M. P., and Ritzwoller, M. H. Surface wave tomography of the western United States from ambient seismic noise: Rayleigh
251 and Love wave phase velocity maps. *Geophysical Journal International*, 173(1):281–298, 2008. doi: 10.1111/j.1365-246X.2008.03720.x.
- 252 Lobkis, O. I. and Weaver, R. L. On the emergence of the Green’s function in the correlations of a diffuse field. *J. Acoust. Soc. Am.*, 110(6):7,
253 2001. doi: 10.1121/1.1417528.
- 254 Margerin, L., Planès, T., Mayor, J., and Calvet, M. Sensitivity kernels for coda-wave interferometry and scattering tomography: Theory and
255 numerical evaluation in two-dimensional anisotropically scattering media. *Geophysical Journal International*, 204(1):650–666, Jan. 2016.
256 doi: 10.1093/gji/ggv470.
- 257 Nakata, N., Gualtieri, L., and Fichtner, A., editors. *Seismic Ambient Noise*. Cambridge University Press, Cambridge, 2019.
258 doi: 10.1017/9781108264808.
- 259 Retailleau, L., Boué, P., Stehly, L., and Campillo, M. Locating Microseism Sources Using Spurious Arrivals in Intercontinental Noise Corre-
260 lations. *Journal of Geophysical Research: Solid Earth*, 122(10):8107–8120, 2017. doi: 10.1002/2017JB014593.
- 261 Schippkus, S., Zigone, D., Bokelmann, G. H. R., and the AlpArray Working Group. Ambient-noise tomography of the wider Vienna Basin
262 region. *Geophysical Journal International*, 215(1):102–117, June 2018. doi: 10.1093/gji/ggy259.
- 263 Schippkus, S., Garden, M., and Bokelmann, G. Characteristics of the Ambient Seismic Field on a Large-N Seismic Array in the Vienna Basin.
264 *Seismological Research Letters*, 91(5):2803–2816, July 2020. doi: 10.1785/0220200153.
- 265 Snieder, R., Wapenaar, K., and Larner, K. Spurious multiples in seismic interferometry of primaries. *Geophysics*, 71:SI111–SI124, 2006.
266 doi: 10.1190/1.2211507.
- 267 Snieder, R., van Wijk, K., Haney, M., and Calvert, R. Cancellation of spurious arrivals in Green’s function extraction and the generalized
268 optical theorem. *Physical Review E*, 78(3):036606, Sept. 2008. doi: 10.1103/PhysRevE.78.036606.
- 269 Steinmann, R., Hadzioannou, C., and Larose, E. Effect of centimetric freezing of the near subsurface on Rayleigh and Love wave velocity in
270 ambient seismic noise correlations. *Geophysical Journal International*, 224(1):626–636, Jan. 2021. doi: 10.1093/gji/ggaa406.
- 271 Wapenaar, K., Fokkema, J., and Snieder, R. Retrieving the Green’s function in an open system by cross correlation: A comparison of ap-
272 proaches (L). *The Journal of the Acoustical Society of America*, 118(5):2783–2786, Nov. 2005. doi: 10.1121/1.2046847.
- 273 Weaver, R. L. Equipartition and retrieval of Green’s function. *Earthquake Science*, 23(5):397–402, Oct. 2010. doi: 10.1007/s11589-010-0738-2.
- 274 Wegler, U. and Sens-Schönfelder, C. Fault zone monitoring with passive image interferometry. *Geophysical Journal International*, 168(3):
275 1029–1033, Mar. 2007. doi: 10.1111/j.1365-246X.2006.03284.x.

276 **Supplementary Material**

277 **S1 Avoiding erroneous group-velocity measurements**

278 One strategy to avoid erroneous group-velocity measurements (Fig. 3) is to carefully select which parts of the correlation functions to measure velocities on. The goal is to avoid all cases where interference occurs and may bias measurements. We propose to make the selection in two steps: first a rough causal/acausal selection based on geometry (this is already sufficient in the case of a stronger boundary source contribution), and second a windowing function around expected arrival times, which is necessary if the isolated source causes the stronger contribution.

283 In a first step, we select the line perpendicular to the line connection \mathbf{r}_M and \mathbf{r}_N and going through \mathbf{r}_M (dashed grey line in Fig. S1). West of this line, we measure group travel times on the acausal part of the correlation functions, and East of the line on the causal part. Because the correlation wavefield contribution emerging from \mathbf{r}_N emerges at negative lapse time $\tau(\mathbf{r} = \mathbf{r}_N) = -|\mathbf{r}_M - \mathbf{r}_N|/c$, there can be no interference to the West of the defined line.

287 To the East of the line, where we measure on the causal part of the correlation function, the resulting errors depend on which contribution has higher amplitude. In the case of a higher contribution by the boundary sources (Fig. S1b), we have avoided all measurement errors except for stations very close to \mathbf{r}_M . These remaining errors occur for stations where $|\mathbf{r} - \mathbf{r}_M| \leq w$, with w the width of the wavelet, due to interference of causal and acausal parts of the correlation functions. Station pairs with distances shorter than a few wavelengths are commonly excluded in studies of seismic interferometry for this exact reason.

293 For the case of a stronger isolated source contribution (Fig. S1a), a circle of correct velocity measurements emerges to the East of the line, because this contribution propagates through the circle at negative lapse times. Because we pick at positive lapse times on this side, we pick the undisturbed contribution by the boundary sources. Outside of this circle and up to the defined line, measurements are affected by the contribution of the isolated source, because it has higher amplitudes.

298 A second criterion helps avoid those remaining measurement errors. We define a symmetric windowing function around the master station's location \mathbf{r}_M of expected arrival time windows and pick only within this windowing function (Fig. S2). We choose the half-width of the Ricker wavelet as the window width. In practice, due to unknown velocity structure, a wider windowing function would be needed. We show the impact of the narrow windowing function to illustrate the best-case scenario one can reach with only a windowing function. The case of a stronger isolated noise source (Fig. S2) approaches the measurement errors one finds for a weaker isolated noise source (Figs. 3b and S2b).

305 Finally, if we combine the two criteria, we avoid velocity measurement errors for all station pairs except the stations near \mathbf{r}_M , as described above (Fig. S3).

307 A different strategy may be to define the windowing function around the isolated noise source instead of the master station. Still, one would need a two-step approach and this would require more precise knowledge of the isolated source location. The strategy proposed above relies on the fact that the isolated source contribution is asymmetric, whereas the boundary source contribution is symmetric. If this is violated, a different strategy is necessary.

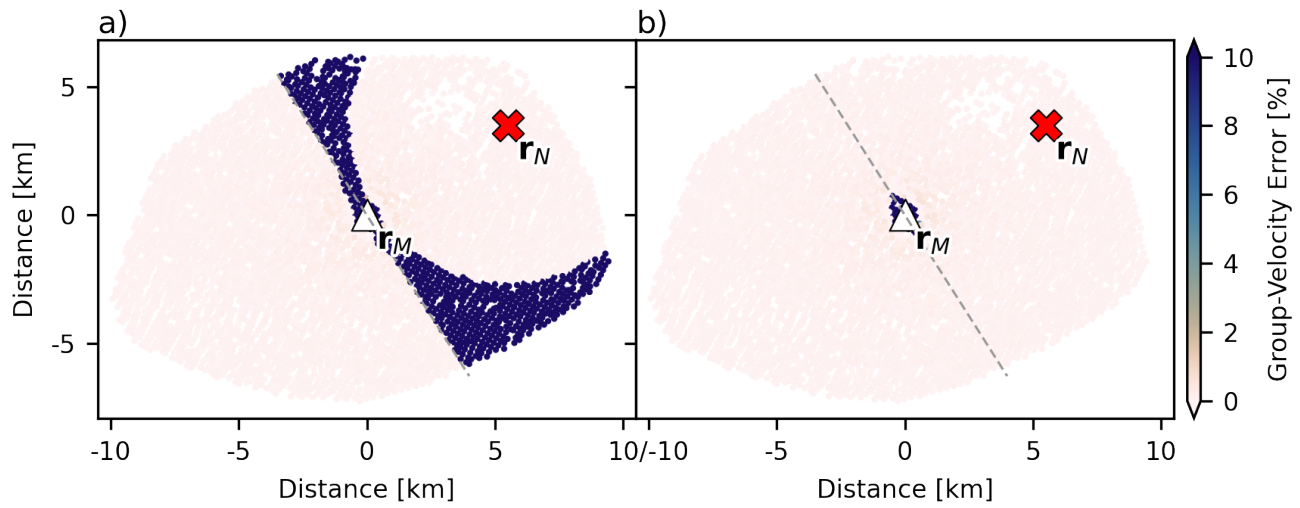


Figure S1 Same as Figure 3 when measuring travel times only on the causal part of correlation functions for stations to the East the dashed line, and only on the acausal part for stations to the West of the dashed line.

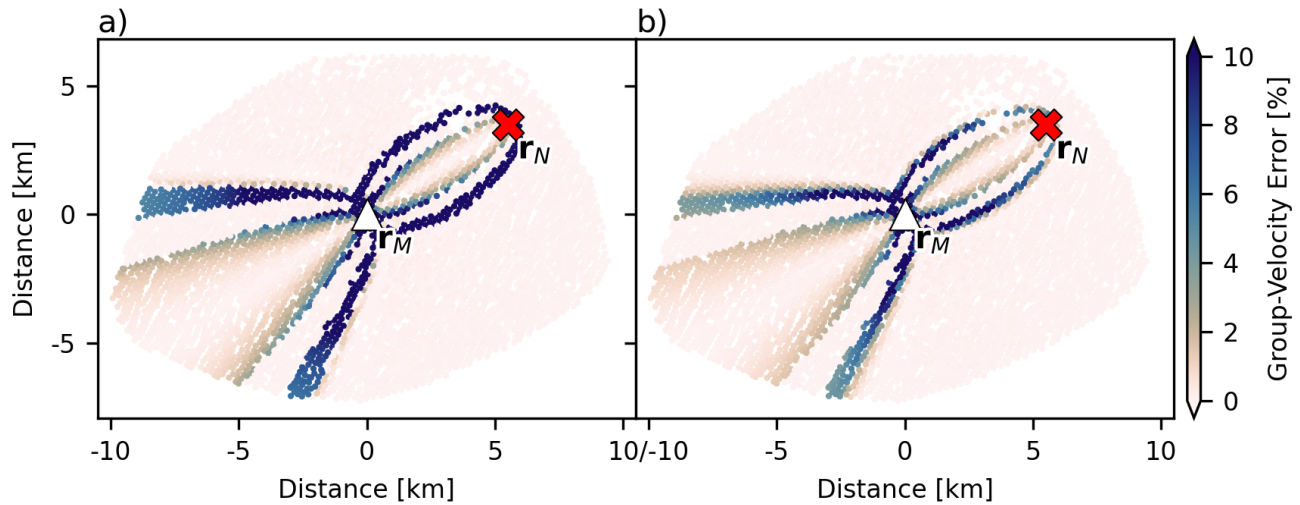


Figure S2 Same as Figure 3 when limiting measurements to an expected arrival window.

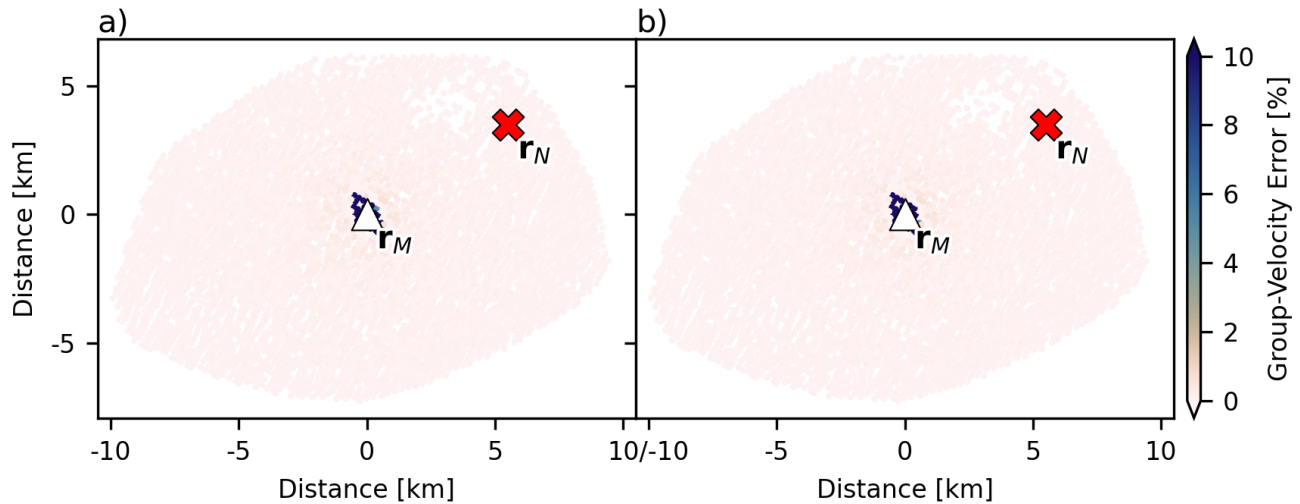


Figure S3 Same as Figure 3 when combining the causal/acausal selection (Fig. S1) and the windowing function (Fig. S2).

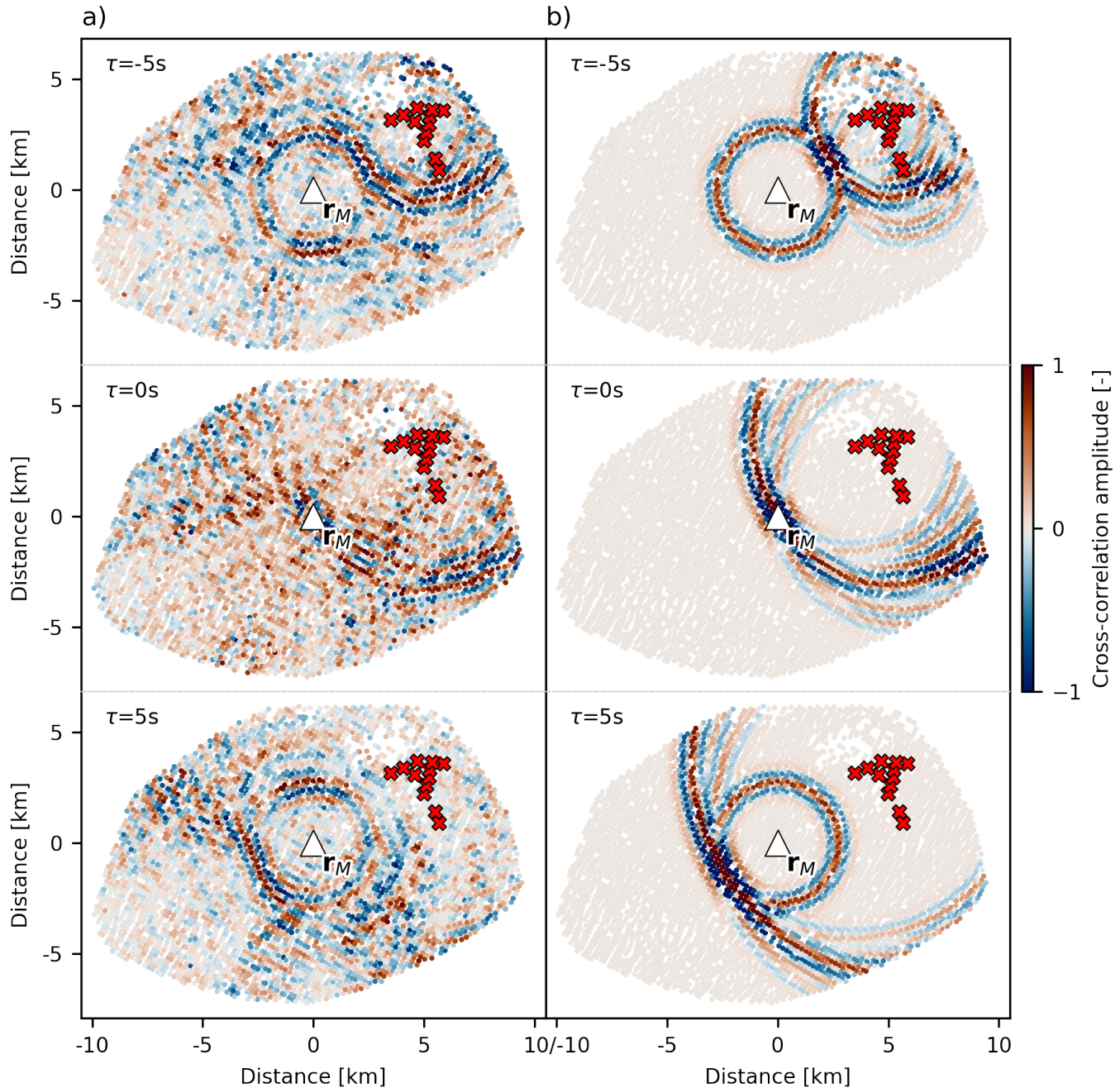


Figure S4 Same as Figure 2 but with all turbines of the wind farm Prottes-Ollersdorf treated as individual sources. Improved fit with the observations compared to Figure 2.